On the structural relations of malachite. I. The rosasite and ludwigite structure families

**Frank Girgsdies* and Malte
Behrens**

Department of Inorganic Chemistry, Fritz-Haber-
Institut der Max-Planck-Gesellschaft, Fara-
dayweg 4–6, Berlin D-14195, Germany

Correspondence e-mail:
girgsdie@fhi-berlin.mpg.de

The crystal structures of malachite $Cu_2(OH)_2CO_3$ and rosasite $(Cu,Zn)_2(OH)_2CO_3$, though not isotypic, are closely related. A previously proposed approach explaining this relation *via* a common hypothetical parent structure is elaborated upon on the basis of group–subgroup considerations, leading to the conclusion that the aristotype of malachite and rosasite should crystallize in the space group *Pbam* (No. 55). An ICSD database search for actual representatives of this aristotype leads to the interesting observation that the structure type of ludwigite $(Mg,Fe)_2FeO_2BO_3$, which is adopted by several natural and synthetic oxide orthoborates $M_3O_2BO_3$, is closely related to the proposed malachite–rosasite aristotype and thus to the malachite–rosasite family of hydroxide carbonates $M_2(OH)_2CO_3$ in general. Relations within both structure families and their analogies are summarized in a joint simplified Bärnighausen tree.

1. Introduction

Synthetic mixed copper/zinc compounds with thermally decomposable anions are interesting materials due to their potential application as catalyst precursors. In particular, mixed hydroxide carbonates are currently used as precursors for the industrial methanol synthesis catalyst $Cu/ZnO/(Al_2O_3)$ (Porta *et al.*, 1988; Waller *et al.*, 1989; Bems *et al.*, 2003; Behrens, 2009). A deeper understanding of the crystal chemistry of such precursor phases may contribute to a more knowledge-based approach towards optimization of catalyst precursors, which prompted us to investigate the possibilities of Cu/Zn substitution in synthetic materials from a more general perspective (Behrens *et al.*, 2009; Behrens & Girgsdies, 2010).

Within the rosasite group of minerals, malachite $Cu_2(OH)_2CO_3$ was the only structurally well characterized member until recently (Wells, 1951; Süsse, 1967; Zigan *et al.*, 1977). This can be ascribed to the fact that the remaining rosasite group minerals crystallize as fibers, not suitable for single-crystal structure determination. Indexing of the powder diffraction patterns also proved difficult, leading to uncertainty concerning unit-cell dimensions and space groups. Consequently, the question of which of the group's members are isostructural to each other remained unsettled for a long time. This situation changed drastically with a series of successful Rietveld refinements by Perchazzi and co-workers for the structures of rosasite, $(Cu,Zn)_2(OH)_2CO_3$, mcguinnessite, $(Mg,Cu)_2(OH)_2CO_3$ (Perchiazzi, 2006), glaukosphaerite, $(Cu,Ni)_2(OH)_2CO_3$, pokrovskite, $Mg_2(OH)_2CO_3$ (Perchiazzi & Merlino, 2006), and chukanovite, $Fe_2(OH)_2CO_3$ (Pekov *et al.*, 2007). All these minerals belong to the rosasite structure type, which is very similar to, but distinct from, the

malachite structure. Malachite thus remains the sole confirmed representative of its own structure type.

In the context of synthetic materials, however, mixed Cu,Zn hydroxide carbonates $(Cu_{1-x}Zn_x)_2(OH)_2CO_3$ usually precipitate in the malachite structure type, apparently with an upper limit of $x \simeq 0.28$. Attempts to further increase the Zn content typically do not lead to synthetic rosasite, which occurs naturally with a Cu:Zn ratio of up to 1:1, but to the formation of phase mixtures containing synthetic zincian malachite and the more zinc-rich mixed hydroxide carbonate, $(Zn,Cu)_5(OH)_6(CO_3)_2$ (synthetic aurichalcite; Millar *et al.*, 1998; Bems *et al.*, 2003; Behrens *et al.*, 2009; Behrens & Girgsdies, 2010).

In our previous work we envisioned the malachite and rosasite structures as alternative distorted derivatives of a common hypothetic parent structure of orthorhombic symmetry (Behrens & Girgsdies, 2010). Here we will describe the malachite–rosasite relation in a more formalized way using group–subgroup relations. As a secondary, highly interesting result we will show that the ludwigite structure type, which occurs in both natural and synthetic oxide orthoborates, $M_3O_2BO_3$, is closely related to the malachite and rosasite structure types. While the similarity of the unit-cell dimensions between the technogene rosasite-type hydroxide carbonate $Fe_2(OH)_2CO_3$ and the borate minerals ludwigite and vonse-

nite has already been noted by Erdös & Altorfer (1976), the detailed structural similarity between the rosasite and ludwigite groups has not been discussed in the literature up to now.

2. Methods

Retrieval of crystal structure data and the database search were carried out using the web interface of the Inorganic Crystal Structure Database (Bergerhoff & Brown, 1987; Belsky *et al.*, 2002), updated October 2010. The unit-cell transformation of the rosasite crystal structure was carried out with *PLATON* (Spek, 2009). Crystal-structure drawings were prepared using *DIAMOND* (Crystal Impact, 2006).

3. Results and discussion

3.1. The malachite–rosasite relation

According to the single-crystal neutron-diffraction study of Zigan *et al.* (1977), malachite crystallizes in the space group $P2_1/a$ (No. 14), with $a = 9.502$, $b = 11.974$, $c = 3.24$ Å, $\beta = 98.75°$. The rosasite crystal structure was determined only recently from X-ray powder diffraction data by Perchiazzi (2006). Starting from the unit-cell parameters of Roberts *et al.* (1986), the structure was successfully refined in the space group $P2_1/a$ (No. 14), with $a = 12.8976$ (3), $b = 9.3705$ (1), $c = 3.1623$ (1) Å, $\beta = 110.262$ (3)°. In later discussions Perchiazzi and co-authors adopted a transformed unit cell, which is still $P2_1/a$ but with $a = 12.2413$ (2), $b = 9.3705$ (2), $c = 3.1612$ (2) Å, $\beta = 98.730$ (3)° (Perchiazzi & Merlino, 2006; Pekov *et al.*, 2007). The latter cell is derived from the originally published one using the transformation matrix [102/0$\bar{1}$0/00$\bar{1}$] and facilitates comparison with the malachite cell. Thus, we follow the second cell choice here, with the atom coordinates taken from Perchiazzi (2006) and transformed according to the cell used in Perchiazzi & Merlino (2006) by applying the above matrix. The *a* axis of malachite corresponds to the *b* axis of rosasite and *vice versa*, which is confirmed by graphical comparison of the respective crystal structures (Fig. 1, top row). The apparent 'swap' of the two axes is the result of crystallographic convention combined with the fact that the monoclinic angle is placed differently in these two otherwise very similar crystal structures. In malachite, the
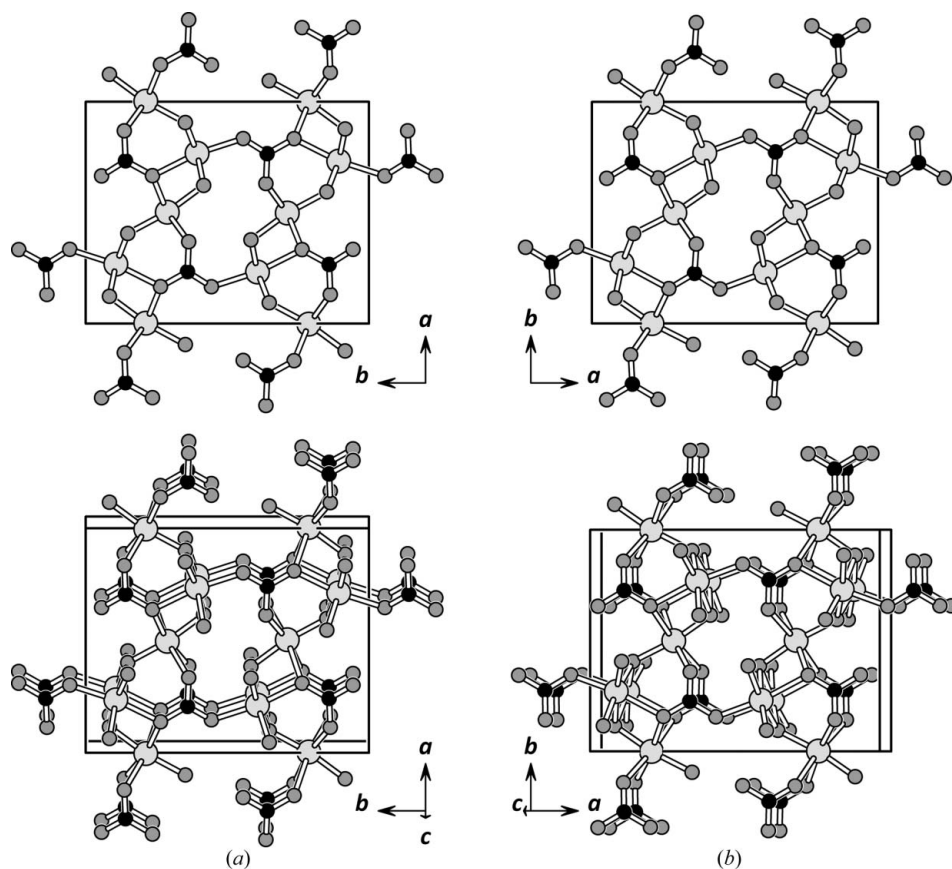
Figure 1
Comparison of the crystal structures of (*a*) malachite and (*b*) rosasite. Projections along the *c* axes (top row) emphasize their close relation, while a view onto the *ab* planes (bottom row) reveals the different placement of the monoclinic angles (metal atoms: light grey, C: black, O: dark grey).

108 Girgsdies and Behrens · Structural relations of malachite. I

Acta Cryst. (2012). B**68**, 107–117

Table 1
Synoptic comparison of unit cells.

Parameters are rounded for convenience, see text for detailed values and references.

	Space group	a (Å)	b (Å)	c (Å)	α (°)	β (°)	γ (°)	V (Å^3)
Malachite	$P12_1/a1$	9.50	11.97	3.24	90	98.8	90	364
Rosasite	$P2_1/b11$	9.37	12.24	3.16	98.7	90	90	358
Ludwigite	$P2_1/b2_1/a2/m$	9.24	12.29	3.02	90	90	90	343

~ 12 Å axis is the monoclinic axis, whereas in rosasite it is the ~ 9 Å axis (Fig. 1, bottom row). As concluded earlier (Behrens & Girgsdies, 2010), the two structure types may be easily envisioned as distortion derivatives of a common orthorhombic parent structure. In a more formal terminology (Megaw, 1973) we consider the malachite and rosasite structure types to be different *hettotypes* of a common *aristotype*, which we will term the 'malachite–rosasite aristotype' (MRA) in the subsequent discussion.

3.2. The space group of the malachite–rosasite aristotype

While no further transformations are necessary for a visual comparison of the malachite and rosasite crystal structures, both a comparison of the atomic coordinates and the search for group–subgroup relations require a common choice of axes for both unit cells. Consequently, we transform one of the two cells into a non-standard setting with a as the monoclinic axis. If we arbitrarily choose to retain the setting $P12_1/a1$ for malachite, then rosasite should be represented in the setting $P2_1/b11$, *i.e.* with the lattice parameters reassigned as $a = 9.3705$ (2), $b = 12.2413$ (2), $c = 3.1612$ (2) Å, $\alpha = 98.730$ (3)°.

If we now speculate that both the malachite and the rosasite structure types can be derived from a common aristotype by symmetry reduction, then there has to be at least one orthorhombic space group of which both $P12_1/a1$ and $P2_1/b11$ are possible *translationengleiche* subgroups. In order to identify this space group, we first consider that the symmetry elements present in the two hettotype structures must be simultaneously present in the aristotype. As the symmetry elements 2_1, a and b are translational ones and thus cause systematic absences in diffraction, we may exploit the reflection conditions to deduce possible space groups for the aristotype. Consultation of Table 3.1.4.1 in Vol. A of *International Tables for Crystallography* (Looijenga-Vos & Buerger, 2006) yields the reflection conditions $0kl: k = 2n, h00: h = 2n, 0k0: k = 2n$ for $P12_1/a1$ and $h0l: h = 2n, h = 2n, 0k0: k = 2n$ for $P2_1/b11$. By combining these conditions, we arrive at the diffraction symbol $Pba-$, with $Pba2$ (32) and $Pbam$ (55) as possible space groups. Among these, only $Pbam$ actually contains all the required symmetry elements, while $Pba2$ is missing the 2_1 screw axes. By consulting ch. 2.3 of Vol. A1 of *International Tables for Crystallography* (Wondratschek & Aroyo, 2006) we are able to verify that both $P12_1/a1$ and $P2_1/b11$ are indeed maximal *translationengleiche* subgroups of $Pbam$. Consequently, it can be concluded that the aristotype of malachite and rosasite must crystallize in the space group $Pbam$.

3.3. Searching for MRA representatives

Next we checked whether the proposed MRA is hypothetical or if representatives of this structure type are known. We searched the ICSD database for entries which would fulfill the following conditions:

(i) elements C and O present (as required for carbonates),

(ii) space group No. 55 (*Pbam* in any setting),

(iii) cell volume 300–400 Å^3 (malachite has $V \simeq 364$ Å^3, rosasite $\simeq 358$ Å^3).

Despite the rather broad search criteria, the search produced zero hits. We conclude that no representative of the MRA has been described so far. Next we tried to find isotypic nitrates. However, modifying the search conditions accordingly (*i.e.* elements N and O must be present) again produced no hits. Finally, we considered that orthoborates could also be isotypic to carbonates. Thus, the search criteria were modified again so that elements B and O had to be present in the structure. This time 42 matching entries were found, all of which turned out to belong to the ludwigite structure type, with the generalized stoichiometry $M_3O_2BO_3$. While there is clearly a discrepancy in the number of cations per formula unit between $M_2(OH)_2CO_3$ and $M_3O_2BO_3$, the close correspondence in both anion count and unit-cell dimensions [*e.g.* $a = 9.2411$ (6), $b = 12.2948$ (9), $c = 3.0213$ (3) Å for ludwigite $(Mg,Fe)_2FeO_2BO_3$; Irwin & Peterson, 1999] suggest that the ludwigite structure type could be related to the hypothetical MRA and thus to the malachite and rosasite types (Table 1).

3.4. Comparison of the ludwigite structure with the malachite–rosasite family

In order to compare the borate and carbonate structures two approaches can be followed. The supposed link between the malachite and rosasite types is the MRA, which also seems to be related to the ludwigite structure type. As no actual crystal structures of the MRA structure type are known, a corresponding model may be built to verify the suspected connection between the carbonate and borate structures. Alternatively, the existing structures can be compared without explicit construction of an intermediate MRA model. Both approaches have merits and drawbacks. To build a model of the MRA structure lattice parameters and relative atomic coordinates are needed to combine them with the symmetry of the space group *Pbam*. As both malachite and rosasite are equally related to the MRA, we could start with the values of either structure. Alternatively, the corresponding parameters of both structures can be averaged. In any case we need to idealize these starting values by imposing the symmetry restrictions of the target space group *Pbam* onto the structure (see §3.5). Thus, this approach could be criticized as being biased towards the anticipated result. Therefore, we will first pursue the strategy of comparing one existing carbonate structure with ludwigite, and construct the MRA model afterwards. A slight weakness of the latter approach is that the malachite and rosasite structures differ from ludwigite in

symmetry, making it necessary to (implicitly or explicitly) include the intermediate step *via* the hypothetical MRA in the formal description of the relation, making the argumentation more cumbersome. As malachite and rosasite are related to ludwigite *via* the MRA, both structures should be equally suitable for this comparison. For practical reasons, however, we chose malachite because its hydrogen positions have been determined experimentally, while such information is currently unavailable for any rosasite-type compound.
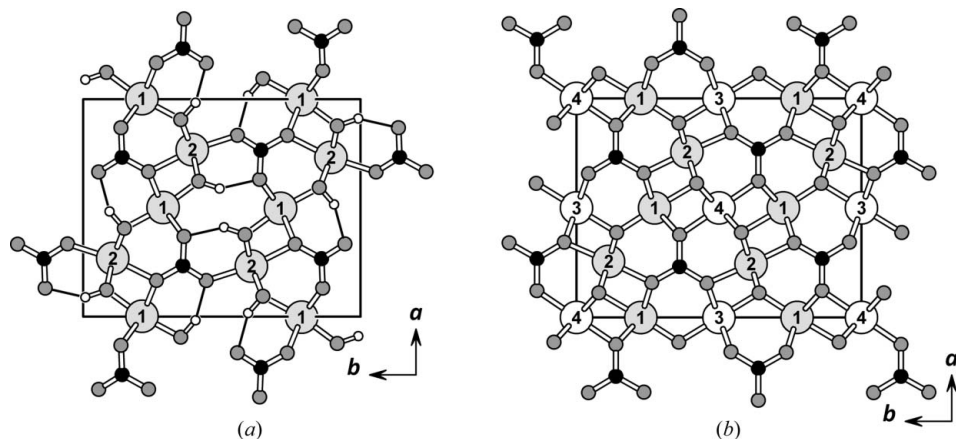
A visual comparison of the malachite and ludwigite crystal structures seen along their respective *c* axes (Fig. 2) demonstrates that their topologies indeed look very similar: all non-H positions in malachite have corresponding counterparts in ludwigite. However, ludwigite contains two additional metal sites (emphasized as white spheres in Fig. 2) which are vacant in malachite. Compared with the two common metal sites,

these 'additional' metal sites have a higher symmetry (..2/*m* versus ..*m*) and thus lower multiplicity. As a consequence, the two 'additional' sites correspond to one of the three metal atoms in the generalized formula $M_3O_2BO_3$.

While Fig. 2 already hints at the type of relation between the ludwigite and malachite structures, it becomes clearer if we modify the structure diagrams to guide the eye. By selectively omitting bonds around both the 'additional' metal atoms in ludwigite and the H atoms in malachite, we emphasize the remaining common structural framework. At the same time, the difference becomes obvious: each 'additional' metal atom in ludwigite corresponds to a pair of symmetry-related H atoms in malachite (Fig. 3).

In order to summarize the relation between the carbonate and borate structures, we now turn from malachite to the higher-symmetry hypothetical MRA. The ludwigite structure type can be obtained from the MRA by replacing two symmetrical pairs of hydrogen sites with additional metal sites on the hydrogen pair's center of gravity (center of inversion). While the MRA and the ludwigite type share the same symmetry (same space group, corresponding unit-cell parameters), they are not isotypic due to the partially incongruent occupation of Wyckoff sites. If we ignore the H atoms, as often done in the discussion of structure types, we may state that all the occupied Wyckoff sites of the MRA would form a *subset* of the occupied Wyckoff sites present in the ludwigite type. Thus, we could call the MRA the *parent type* and the ludwigite structure the corresponding *interstitial type* according to the definitions of Bergerhoff *et al.* (1999). Alternatively, we may address the ludwigite type as a *stuffed variant* of the MRA, and the MRA as *vacancy variant* of the ludwigite structure following the terminology used by Bärnighausen (1980). It should be noted that inclusion of the H atoms into the discussion makes the situation only slightly more complex. In this case both the MRA and the ludwigite type could be regarded as two alternative interstitial types derived from a common parent type. A more detailed discussion of the nomenclature issues concerning interstitial structure types is given in *Appendix A*.

Figure 2
Comparison of the crystal structures of (*a*) malachite and (*b*) ludwigite, seen along the [001] direction. Metal sites which are common to both structures are shown in light grey and labeled 1 and 2. Those ludwigite metal sites which are vacant in malachite are shown as white spheres and labeled 3 and 4. Additionally, the H atoms of malachite are shown (small white spheres), including hydrogen bonds. Owing to their crystal chemical correspondence, C and B atoms are both depicted in black.
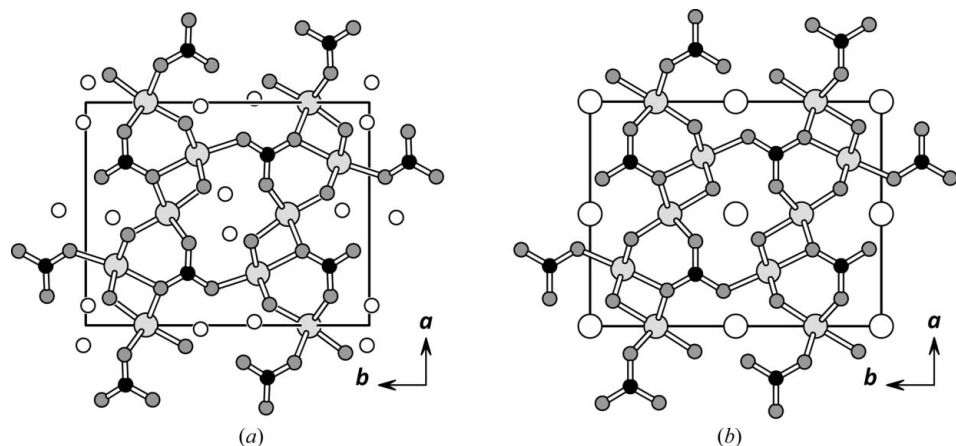
Figure 3
A suggestive way of depicting the structures of (*a*) malachite and (*b*) ludwigite, emphasizing both similarities and differences at the same time (see text for details). It should be noted that a corresponding comparison of rosasite (if the hydrogen positions were known) or the MRA (if a real compound of this type existed) with ludwigite would probably result in an almost identical picture.

3.5. Comparison of atomic coordinates and construction of an MRA model structure

After having compared the carbonate and borate structures visually in the x,y projection, we can now proceed with evaluating the implications of the symmetry increase from the malachite and rosasite structures to the proposed MRA for the z component of the atomic coordinates. If the malachite and rosasite structures are projected along their respective a and b axes (not shown here, but see e.g. Fig. 8 of Behrens & Girgsdies, 2010), we see that the z displacements of the atoms from a common idealized symmetry are quite pronounced. Still, both structures apparently share a pseudo-symmetry in which all atoms would be aligned in sets of planes parallel to the ab plane. This observation is compatible with the fact that the space group $Pbam$ of the MRA and ludwigite structures includes mirror planes perpendicular to c, which are lost upon symmetry reduction to $P12_1/a1$ or $P2_1/b11$. Consequently, the z coordinates of all atoms in the MRA structure should be restricted to the special values 0 or $\frac{1}{2}$. Based on these preliminary considerations, we can now compare the crystal structures numerically with respect to their atomic coordinates. It should be noted that several transformations (unit-cell transformations, permitted origin shifts, choice of symmetry-equivalent positions from atomic orbits) may be required to obtain comparable sets of coordinates. Fig. 5 lists the corresponding coordinates of malachite, rosasite, ludwigite and $Cu_2AlO_2BO_3$ (a ludwigite derivative which will be discussed below, §3.6), and details on the transformations applied are given in Appendix B1.

In a next step the coordinates are compared quantitatively for pairs of related structures. The results of these comparisons are collected in Appendix B2. First, the differences between the relative atomic coordinates of the two structures under comparison are given in Table 2. However, since the three unit-cell axes differ significantly in length, the relative displacement values in the x, y and z directions should be considered of different importance. Hence, the relative displacements are also converted into approximate absolute values by multiplication with the corresponding axis lengths. For simplicity, the unit-cell measures of the ludwigite structure are used in all cases. From these comparisons, it can now be seen that all the listed crystal structures have very similar relative atomic coordinates in the x and y directions. The corresponding absolute discrepancies rarely exceed 0.2 Å. In contrast, much larger relative differences can be found in the z direction. The corresponding absolute values demonstrate that this effect is not only caused by the significantly shorter length of the c axis relative to a and b. Within the malachite–rosasite and ludwigite families, the z direction, if not restricted by symmetry, apparently represents the largest degree of freedom, with differences of the order 0.4−0.5 Å being quite common. If we consider the fact that malachite, rosasite and $Cu_2AlO_2BO_3$ contain Cu^{2+} we might suspect that the Jahn–Teller distortion of the CuO_6 octahedra could contribute significantly to this effect. For example, the shorter equatorial Cu—O bonds in malachite vary between 1.90 and 2.11 Å, with

an average length of 1.98 Å, while the longer axial distances vary between 2.37 and 2.64 Å, with an average of 2.47 Å. In other words, while the ranges of values for equatorial and axial bonds span 0.21 and 0.27 Å, the difference between the average axial and equatorial values is as large as 0.49 Å. Furthermore, the Jahn–Teller elongated axes of the octahedra show different orientation patterns in malachite and rosasite (Behrens & Girgsdies, 2010) for a more detailed discussion). However, due to the specific inclination of the Jahn–Teller axes relative to the base vectors of the respective unit cells, this type of displacement should affect all the directions of the crystal structures to a similar degree. Consequently, other factors must contribute to the pronounced z displacements. We suppose that a significant part of the z deviations in malachite and rosasite result from the distortive potential of the hydrogen bonds (see §3.6), which are absent in ludwigite and its hettotypes. This assumption is supported by the fact that in the comparison between $Cu_2AlO_2BO_3$ and ludwigite, the observed deviations are much smaller despite the presence of Cu^{2+} and the absence of symmetry restrictions for the z coordinates in $Cu_2AlO_2BO_3$.

Finally, we construct an explicit structure model for the MRA with the resulting coordinates presented in Fig. 5. The unit-cell parameters a, b and c, as well as the x and y coordinates, are obtained by averaging the corresponding parameters from the malachite and rosasite structures, while the unit-cell angles and z coordinates are assigned special values resulting from the symmetry restrictions of the space group $Pbam$. To obtain the MRA z coordinates, values of 0 or $\frac{1}{2}$ were assigned if the corresponding malachite/rosasite values were in the ranges $-\frac{1}{4} < z < \frac{1}{4}$ or $\frac{1}{4} < z < \frac{3}{4}$. Despite the pronounced displacements from the ideal pseudo-symmetry observed in the z direction for both malachite and rosasite (see Appendices B1 and B2), this assignment procedure yields the same results starting from the parameters of either structure. Furthermore, the resulting z coordinates also agree with those of ludwigite, thus confirming the originally proposed relation between MRA and ludwigite.

3.6. Building a structure family tree

So far we have discussed the malachite–rosasite relation via the common aristotype MRA, as well as the structural connection between the MRA and the ludwigite type. For a more general treatment it is worthwhile to also include derivative structures within the ludwigite family into the discussion. Several hettotypes of the ludwigite type have been reported in the literature. For example, the synthetic copper-containing derivatives $Cu_2MO_2BO_3$ (M = Al, Ga, Fe; Hriljac et al., 1990; Schaefer & Bluhm, 1995) are representatives of a monoclinically distorted ludwigite type crystallizing in the space group $P2_1/a$ (No. 14), with the ~ 12 Å axis as the monoclinic axis. Thus, the relation between the $Cu_2AlO_2BO_3$ and ludwigite types is analogous to the relation between the malachite structure and the MRA. In other words we may state that (again ignoring the H atoms) the $Cu_2AlO_2BO_3$ type represents a *stuffed variant* of the malachite structure, which

can be verified by a comparison of the corresponding atomic sites (*Appendices B*1 and *B*2). Hence, one could ask now if there is also a rosasite-analogous hettotype of ludwigite. According to our research using the ICSD database, this does not seem to be the case. However, there are two other ludwigite hettotypes which provide an indirect link in this context. The synthetic compound $Ni_5SnO_4(BO_3)_2$ crystallizes in the space group *Pnam* (No. 62), with a doubled *c* axis compared with the ludwigite unit cell (Bluhm & Müller-Buschbaum, 1989*a*). Doubling of the unit cell is a consequence of cation ordering in conjunction with the 5:1 ratio between divalent and tetravalent metal ions. The same structure type is also found for $Ni_5HfO_4(BO_3)_2$ (Bluhm & Müller-Buschbaum, 1989*b*) and the magnetically ordered low-temperature phase of $Fe_3O_2BO_3$ (Mir *et al.*, 2006; Bordet & Suard, 2009). For $Cu_5SnO_4(BO_3)_2$ (Schaefer & Bluhm, 1994), however, a monoclinic distortion perpendicular to the ∼ 9 Å axis occurs in addition to the doubling of the *c* axis, leading to space group No. 14 (non-standard setting $P2_1/b11$ with our choice of coordinate system). While it seems only natural to explain the $Cu_5SnO_4(BO_3)_2$ structure as being derived from the ludwigite type *via* the intermediate $Ni_5SnO_4(BO_3)_2$ type, we can also take an alternative point of view. For the sake of argument, we may as well derive the $Cu_5SnO_4(BO_3)_2$ type by a monoclinic distortion of the simple ludwigite cell, followed by subsequent doubling of the *c* axis. In the latter case, the intermediate structure type is hypothetical, but it is interesting to note that it would represent a monoclinic ludwigite derivative with a monoclinic axis of ∼ 9 Å and thus be an analog of the rosasite type. In other words, we may describe the $Cu_5SnO_4(BO_3)_2$ type as a *stuffed variant* of a rosasite-type structure with a doubled unit-cell.

A convenient way to summarize group–subgroup relations is to depict them in a Bärnighausen tree (Bärnighausen, 1980; Müller, 2004). One minor complication in this respect is that the relation between the malachite–rosasite and the ludwigite families of structures can only be treated indirectly. For example, the ludwigite type and the MRA have the same space group and corresponding unit cells, therefore, their relation is not a group–subgroup one. Owing to their equivalence in symmetry, both structure types will occupy the same place in a Bärnighausen diagram. Of course it would be possible to draw two separate trees for the two structure families. However, owing to their close structural relation and the rather complementary distribution of known representatives, we find it more enlightening to chart the two families on a common tree to point out analogies and gaps (Fig. 4). Complete Bärnighausen trees usually include tables of atomic coordinates and Wyckoff sites of the charted structures (see *e.g.* Müller, 2004). For reasons of space restriction we have not included these tables in Fig. 4, but show accordingly formatted tables in Fig. 5 (*Appendix B*1) to complement the tree. However, we have not included all the structures from the tree in the appendix as a thorough treatment of all ludwigite hettotypes is beyond the scope of this work.

An important part of the group–subgroup relations of crystal structures are the corresponding relations between the

Wyckoff positions (Müller, 2006). Thus, the compatibility of Wyckoff positions may provide a valuable test for a proposed structure relation. In the current case, however, the Wyckoff relations are relatively uninformative unless the coordinate values are explicitly included into the considerations. All atoms of the malachite and rosasite structure types are located on general positions, 4*e*. Thus, they could be related to several Wyckoff sites in *Pbam*: 4*e*/4*f* (..2), 4*g*/4*h* (..*m*), or even 8*i* (if two independent 4*e* sites in $P12_1/a1$ or $P2_1/b11$ would become symmetry equivalent in *Pbam*). Positions leading to 4*e*/4*f* (..2) in *Pbam* should have *x* and *y* values close to 0 or $\frac{1}{2}$, which is not observed for any malachite or rosasite atom position (*Appendix B*1). Correspondingly, a visual inspection (Fig. 1, top row) confirms that none of the atoms seem to be located on a site with a twofold rotational pseudo-symmetry. Sites corresponding to 4*g*/4*h* (..*m*) in *Pbam* are expected to have *z* values close to 0 or $\frac{1}{2}$ in $P2_1/a$. Although this is barely apparent from the corresponding malachite and rosasite coordinate values listed in Table 2, the procedure described in §3.5 demonstrates that this is indeed the Wyckoff relation which is relevant for the relation between malachite and rosasite with their common aristotype. Finally, the 'interstitial' metal atoms in the ludwigite type (*Pbam*) are located on 2*a* and 2*d* (..2/*m*) sites, which correspond to the 2*a* and 2*b* ($\bar{1}$) sites in the lower

$$P\,b\,a\,m\,\,(55)$$

ludwigite

(*MRA*)

*t*2   *k*2 | **a, b**, 2**c**   *t*2

$P\,1\,2_1/a\,1\,\,(14)$ $P\,n\,a\,m\,\,(62)$ $P\,2_1/b\,1\,1\,\,(14)$

$Cu_2AlO_2BO_3$ $Ni_5SnO_4(BO_3)_2$

malachite   rosasite

*t*2   *i*2 | **a, b**, 2**c**

	a (Å)	*b* (Å)	*c* (Å)	
ludwigite	9.24	12.29	3.02	
$Cu_2AlO_2BO_3$	9.37	11.78	3.07	$\beta = 97.7°$
$Ni_5SnO_4(BO_3)_2$	9.30	12.28	6.09	
$Cu_5SnO_4(BO_3)_2$	9.50	12.10	6.36	$\alpha = 93.3°$
malachite	9.50	11.97	3.24	$\beta = 98.8°$
rosasite	9.37	12.24	3.16	$\alpha = 98.7°$

$P\,2_1/b\,1\,1\,\,(14)$

$Cu_5SnO_4(BO_3)_2$

Figure 4
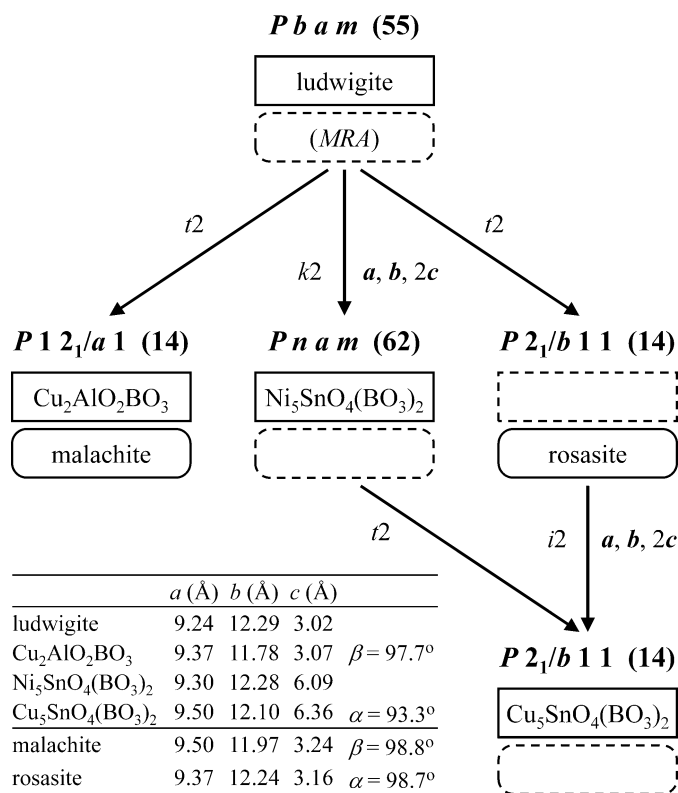A combined simplified Bärnighausen tree for the ludwigite structure type family (rectangular boxes) and the malachite-rosasite family (rounded boxes). Structure types without known representatives are shown in dashed outlines. All space-group symbols are chosen according to a common orientation of the unit cells. The corresponding atom sites to complement the simplified tree are given in Fig. 5 (*Appendix B*1).

symmetry ($P2_1/a$) $Cu_2AlO_2BO_3$ type and, correspondingly, the malachite structure (although unoccupied in the latter). In the rosasite type, the empty 'interstitial' sites are 2a and 2d ($\bar{1}$), respectively, because of the different orientation of axes in the original setting (monoclinic axis b). In summary, all Wyckoff relations can be shown to be compatible with the proposed symmetry relations.

The combined tree of the malachite–rosasite and ludwigite structure families may now serve as a roadmap to discover trends and point out gaps in our current knowledge. For example, it nicely illustrates the aforementioned possibility to derive $Cu_5SnO_4(BO_3)_2$ from the ludwigite type via two alternative pathways, using either the $Ni_5SnO_4(BO_3)_2$ type or a hypothetical rosasite analogous structure type as possible intermediates. Thus, one may now ask whether it could be possible to synthesize a ludwigite derivative analogous to rosasite. It is also worth noting that the $Cu_5SnO_4(BO_3)_2$ structure could be derived from ludwigite via a third subgroup chain, which can be recovered e.g. by using the SUBGROUPGRAPH tool of the Bilbao Crystallographic Server (Ivantchev et al., 2000). In this case the intermediate retains Pbam symmetry, but has a doubled c axis. However, a corresponding ICSD search yields no carbonate, nitrate or borate crystal structures of this particular type. Hence, this additional but empty branch is omitted from the simplified Bärnighausen tree in Fig. 4. Another consideration which follows from the tree is that the distribution of known representatives suggests that the occurrence of the lower monoclinic symmetry could be associated with the presence of the Jahn–Teller ion Cu^{2+} in the structure. The only known exceptions from this trend are the two rosasite-type minerals pokrovskite, $Mg_2(OH)_2CO_3$, and chukanovite, $Fe_2(OH)_2CO_3$. Thus, the next obvious question would be why a compound containing exclusively metal ions with a symmetric d-electron configuration like $Mg_2(OH)_2CO_3$ does not crystallize in the higher-symmetry MRA structure. In this context it is worth-while noting that the crystal structure of pokrovskite is apparently non-stoichiometric, with statistical Mg^{2+} vacancies balanced by additional protons (Perchiazzi & Merlino, 2006). A similar, but less pronounced, non-stoichiometry was also indicated for chukanovite (Pekov et al., 2007). However, whether cation non-stoichiometry might be characteristic for copper-free rosasite-type structures must remain an open question until more evidence is available. Finally, we would like to point out that Liu et al. (2009) have recently reported two possible high-pressure phase transitions of malachite, although the data quality did not permit details about the structural changes to be extracted. Thus, one may reasonably propose the MRA structure as a model to represent a high-pressure phase of malachite.

As the MRA structure type seems to be non-existent, at least under ambient conditions, one may look for factors which could destabilize such a structure by making it energetically unfavorable. A good candidate for such a factor could be hydrogen bonding. When the crystal structures of malachite and rosasite are viewed along their respective a and b axes (cf. e.g. Fig. 8 in Behrens & Girgsdies, 2010), it is

apparent that in addition to the monoclinic distortion of the unit cell, the positions of the metal atoms and carbonate ligands are displaced significantly with respect to the ideal MRA mirror plane. Furthermore, the carbonate groups are tilted with respect to this hypothetical plane. These distortions are also reflected in the relatively large deviations of the z values from the ideal pseudosymmetry discussed in §3.5. At least in the malachite structure these distortions seem to be the result of hydrogen-bond interactions. While the hydrogen positions have not been located in rosasite, there is little doubt that the same mechanisms would also apply. If we now consider the possibilities for hydrogen bonding in the hypothetical MRA structure, we find that the H atoms should be located on mirror planes (..m positions), together with their corresponding donor O atoms. The next hydrogen-bond acceptor atoms would then lie on the two neighboring ($z \pm \frac{1}{2}$) mirror planes, at equal distances. Thus, for symmetry reasons hydrogen bonding could only occur in a symmetrically bifurcated Y-shaped geometry. Even without using theoretical calculations, it seems likely that such a perfectly symmetric bonding mode should be less favorable than asymmetric, and thus more directed, hydrogen bonds. Consequently, we assume that hydrogen bonding is a key factor in stabilizing the monoclinic rosasite structure relative to the symmetric MRA, even in the absence of Jahn–Teller ions such as Cu^{2+}. In contrast, H atoms (and thus hydrogen bonds) are absent in the ludwigite family. Hence, most members crystallize in ortho-rhombic space groups with mirror planes, except for those examples which contain the Jahn–Teller ion Cu^{2+}.

3.7. Substitution of non-H atoms with hydrogen pairs – a more generally applicable concept?

Analogous to the 'guide to the eye approach' taken to depict the close structural relation in Fig. 3, we can also suggest a way to rewrite the chemical formulae of $M_2(OH)_2CO_3$ and $M_3O_2BO_3$ to better represent this relation. By choosing the notations $M_2[H_2]^oO_2CO_3$ and $M_2[M]^oO_2BO_3$, we emphasize the common structural framework, with $[]^o$ representing the variably occupied octahedral spaces inside this framework. Consequently, we are now able to describe the malachite–rosasite and ludwigite families as representing two special cases ($A = H_2$, $X = C$) and ($A = M$, $X = B$) of a more general notation $M_2[A]^oO_2XO_3$.

While the substitution of metal atoms with pairs of H atoms and vice versa is a mere formalism in the malachite–rosasite to ludwigite comparison, we emphasize that there is at least one example in the literature in which this type of substitution is much less formal. A close structural relation exists between $H_2U_3O_{10}$ [$P\bar{1}$, $a = 6.802$ (5), $b = 7.417$ (16), $c = 5.556$ (5) Å, $\alpha = 108.5$ (4), $\beta = 125.5$ (1), $\gamma = 88.2$ (2)°; Siegel et al., 1972] and CuU_3O_{10} [$P\bar{1}$, $a = 6.516$ (5), $b = 7.614$ (2), $c = 5.615$ (7) Å, $\alpha = 109.464$ (9), $\beta = 125.18$ (2), $\gamma = 89.993$ (3)°; Dickens et al., 1993]. Although the positions of the H atoms in $H_2U_3O_{10}$ have not been determined directly, it has been inferred from short oxygen–oxygen distances and bond-strength sum calculations that they should occupy the same octahedral void as the Cu

atom in CuU_3O_{10} (Siegel *et al.*, 1972). Although we are currently not aware of further examples, it seems not unlikely that structural relations *via* metal *versus* hydrogen-pair substitutions, formal or not, could be more widespread than is currently recognized.

4. Summary and conclusions

We have shown that the malachite and rosasite structures represent two alternative hettotypes of a common aristotype. The MRA has orthorhombic symmetry, space group *Pbam* (No. 55), albeit no actual representatives of this hypothetical aristotype have been reported so far. The MRA structure is in turn closely related to the ludwigite structure type. The ludwigite type can be obtained from the MRA by replacing two crystallographically independent, inversion-symmetric pairs of hydrogen sites located around octahedral voids with two additional metal sites on the respective centers of symmetry. It has been shown that the application of group–subgroup relations can indicate new hypothetical structure types, which may turn out to be valuable 'missing links' in uncovering previously unconsidered structural relations, even between long-known mineral structure types.

APPENDIX *A*
On the nomenclature of structure types with occupied interstitial sites

When trying to describe the relation between the ludwigite structure type and the hypothetical MRA we were confronted with the dilemma that the official nomenclature recommendations do not seem to cover the case under discussion. The Subcommittee on the Nomenclature of Inorganic Structure Types of the IUCr Commission on Crystallographic Nomenclature has published recommendations on the nomenclature of inorganic structure types (Lima-de-Faria *et al.*, 1990). This publication defines several special terms to describe various kinds and degrees of relations between crystal structures. Among these, the only definition which deals with the filling of structures with additional interstitial atoms is §1.7: '***Interstitial (or 'stuffed') derivatives** represent compounds in which unoccupied 'interstitial' sites (voids) of the basic structure are (progressively) filled by atoms in the derivative structure. In general, the relationship between the unfilled parent (basic) structure and the derivatives based on filling one specific interstitial site approaches homeotypism*' (Lima-de-Faria *et al.*, 1990). We would like to emphasize that this definition applies the terms *basic structure* to the unfilled and *derivative structure* to the filled structures. The terms *basic structure* and *derivative structure* are, however, typically used in the context of group–subgroup relations since the publication of Buerger's *Derivative Crystal Structures* (Buerger, 1947), and thus are considered to be synonyms of the terms *aristotype* and *hettotype*, coined later by Megaw (1973). As a consequence, we conclude that the IUCr definition of *interstitial* (or *'stuffed'*) *derivatives* seems to imply the existence of a group–subgroup

relation between the unfilled and filled structures. We argue, however, that the filling of a crystal structure type should not be associated *a priori* with a particular type of symmetry relation. As can be easily envisioned, the occupation of interstitial sites could also leave the symmetry unchanged (as in the case discussed in this work) or even increase the symmetry according to a group–supergroup relation. Thus, it seems to us that the term *interstitial* (or *'stuffed'*) *derivatives* has been defined too narrowly. Cases of filling of interstitial sites under symmetry retention or symmetry increase are neither covered by this definition nor by any other special term defined by Lima-de-Faria *et al.* (1990), except by the rather broadly defined term *homeotypic*.

When Bergerhoff and co-workers published their two-part work *concerning inorganic crystal structure types*, they were apparently confronted with the same dilemma. In the introduction of part one (Bergerhoff *et al.*, 1999), explicit reference is made to the IUCr's nomenclatorial recommendations of Lima-de-Faria *et al.* (1990), summarizing most of the definitions in their own words. The term *interstitial* (or *'stuffed'*) *derivative*, however, is avoided. Instead, the terms *interstitial type* and *interstitial homeotype* are introduced as follows: '*interstitial type: in derivatives, additional Wyckoff positions of the parent structures are (progressively) occupied*' and '*inter-interstitial homeotype: in derivatives, additional Wyckoff positions of the parent structures are (progressively) occupied but derivative and parent structures cannot be traced back to isopointal structures*' (Bergerhoff *et al.*, 1999). Several examples of such *interstitial types* and their corresponding *parent types* are given in both parts of the work (Bergerhoff *et al.*, 1999; Bergerhoff, 2001), in which the *interstitial types* and their corresponding *parent types* share the same symmetry, and the Wyckoff positions of a *parent type* form a subset of the Wyckoff positions of its *interstitial type*. The term *interstitial homeotype*, however, is not detailed or used any further, nor are we aware of any subsequent use in the literature. Unfortunately, it is not readily apparent whether Bergerhoff's terms *interstitial type* and *interstitial homeotype* together were intended to complement, or replace, the IUCr term *interstitial derivative*. In any case, we believe that the introduction of these terms by Bergerhoff *et al.* (1999) is indeed a result of the shortcomings of the IUCr definition. Finally, we would like to point out that Bärnighausen (1980), in the concluding paragraph of his classic work on group–subgroup relations, used the terms *vacancy variant* and *stuffed variant* for corresponding unfilled and filled structure types. We think that this is a very appropriate choice of terms, as they appear to be quite neutral in the sense that they do not seem to imply a specific kind of symmetry relation between the structures, despite the fact that the work was mainly focused on group–subgroup relations.

To conclude this line of thought, we think that an amendment of the IUCr recommendation concerning *interstitial* (or *'stuffed'*) *derivatives* might be warranted. Our suggestion would be to avoid the term *derivative* altogether, and find a definition which is less exclusive with respect to the required type of symmetry relation. The terms *vacancy variant* (of a

114 Girgsdies and Behrens · Structural relations of malachite. I

Acta Cryst. (2012). B**68**, 107–117

structure type) and *stuffed variant* (of a structure type), as introduced by Bärnighausen (1980), could be suitable candidates for an amended terminology. The definition should cover cases of stuffing of a structure type with interstitial atoms under:

(i) symmetry decrease according to a group–subgroup relation,

(ii) symmetry retention, and

(iii) symmetry increase according to a group–supergroup relation.

APPENDIX *B*
Comparison of atom sites

B1. Atom position tables (Fig. 5)

In the following the Wyckoff positions and atomic coordinates of selected crystal structures are given in order to complement the simplified Bärnighausen diagram shown in Fig. 4. In an extension of the usual representation (see *e.g.*

Ludwigite, Pbam

	M: 2a ..2/m	M: 2d ..2/m	M: 4g ..m	M: 4h ..m	O: 4g ..m	O: 4g ..m	O: 4h ..m	O: 4h ..m	O: 4h ..m	B: 4h ..m
a = 9.24 Å	0	$\frac{1}{2}$	0.002	0.240	0.384	0.109	0.850	0.625	0.851	0.274
b = 12.29 Å	0	0	0.280	0.115	0.077	0.142	0.043	0.142	0.237	0.360
c = 3.02 Å	0	$\frac{1}{2}$	0	$\frac{1}{2}$	0	0	$\frac{1}{2}$	$\frac{1}{2}$	$\frac{1}{2}$	$\frac{1}{2}$
	M1	M2	M3	M4	O2	O4	O1	O3	O5	B

Cu₂AlO₂BO₃, P1 2/a 1

	M: 2a $\bar{1}$	M: 2b $\bar{1}$	M: 4e 1	M: 4e 1	O: 4e 1	O: 4e 1	O: 4e 1	O: 4e 1	O: 4e 1	B: 4e 1
a = 9.37 Å	0	$\frac{1}{2}$	−0.007	0.231	0.387	0.106	0.843	0.617	0.831	0.265
b = 11.78 Å	0	0	0.280	0.117	0.075	0.144	0.038	0.133	0.239	0.364
c = 3.07 Å	0	$\frac{1}{2}$	0.040	0.571	0.002	0.041	0.517	0.505	0.587	0.535
β = 97.7°	M2	M3^i	M1	M4^{ii}	O4^{iii}	O1	O2^{ii}	O3^{iii}	O5	B1^i

(i) $\frac{1}{2} - x, \frac{1}{2} + y, -z$; (ii) $-x, -y, -z$; (iii) $\frac{1}{2} + x, \frac{1}{2} - y, z$

Malachite, P1 2₁/a 1

	2a $\bar{1}$	2b $\bar{1}$	Cu: 4e 1	Cu: 4e 1	O: 4e 1	O: 4e 1	O: 4e 1	O: 4e 1	O: 4e 1	C: 4e 1
a = 9.50 Å	0	$\frac{1}{2}$	−0.002	0.232	0.377	0.094	0.834	0.631	0.833	0.266
b = 11.97 Å	0	0	0.288	0.107	0.084	0.148	0.056	0.136	0.236	0.359
c = 3.24 Å	0	$\frac{1}{2}$	−0.108	0.388	−0.140	−0.081	0.631	0.342	0.450	0.473
β = 98.8°	–	–	Cu1	Cu2^i	O5^i	O4^i	O3	O1	O2	C^i

(i) $\frac{1}{2} + x, \frac{1}{2} - y, z$

Rosasite, P2₁/b 1 1

	2a $\bar{1}$	2d $\bar{1}$	Cu: 4e 1	M: 4e 1	O: 4e 1	O: 4e 1	O: 4e 1	O: 4e 1	O: 4e 1	C: 4e 1
a = 9.37 Å	0	$\frac{1}{2}$	0.001	0.230	0.385	0.095	0.845	0.642	0.843	0.275
b = 12.24 Å	0	0	0.290	0.106	0.081	0.146	0.052	0.135	0.231	0.359
c = 3.16 Å	0	$\frac{1}{2}$	0.028	0.384	−0.093	−0.061	0.633	0.511	0.599	0.383
α = 98.7°	–	–	Cu1^i	Me2^i	O5^i	O4^i	O3	O1	O2	C^i

(i) $\frac{1}{2} - x, \frac{1}{2} + y, -z$

MRA model, Pbam

	H: 4g ..m	H: 4g ..m	M: 4g ..m	M: 4h ..m	O: 4g ..m	O: 4g ..m	O: 4h ..m	O: 4h ..m	O: 4h ..m	C: 4h ..m
a ≅ 9.44 Å	0.411	0.017	−0.001	0.231	0.381	0.095	0.840	0.637	0.838	0.271
b ≅ 12.11 Å	0.008	0.095	0.289	0.107	0.083	0.147	0.054	0.136	0.234	0.359
c ≅ 3.20 Å	0	0	0	$\frac{1}{2}$	0	0	$\frac{1}{2}$	$\frac{1}{2}$	$\frac{1}{2}$	$\frac{1}{2}$

Figure 5
Comparative atom position tables for selected compounds from Fig. 4. Additionally, data for an MRA model are listed, with broken lines around the H positions indicating their non-correspondence with the remaining tables (see text for details).

Müller, 2004), the originally published atom labels are listed below each table to facilitate a comparison with the primary data. If symmetry-equivalent positions of the published coordinates had to be chosen for comparability, the corresponding symmetry operation, with respect to the original set of coordinates, is also given. Trivial coordinate adjustments of ±1, however, are not explicitly stated. The atom site columns of all compounds are sorted in such a way that the corresponding sites from different structures are aligned vertically to reflect their respective correspondence.

The coordinates of ludwigite are used as a reference point for the comparisons and are reported as published (Irwin & Peterson, 1999). Apart from selecting the appropriate symmetry-equivalent positions for each atomic orbit, the coordinates of the ludwigite hettotype $Cu_2AlO_2BO_3$ (Hriljac *et al.*, 1990) were not transformed. For malachite, the starting coordinates from Zigan *et al.* (1977) were shifted by $(x + \frac{1}{2}, y, z)$ to be comparable with the ludwigite coordinates (see *e.g.* Parthé & Gelato, 1984, concerning permitted origin shifts). The original rosasite coordinates (Perchiazzi, 2006) were transformed using $(a + 2c, -b, -c)$ following Perchiazzi & Merlino (2006), then further transformed into the non-standard setting $P2_1/b11$ using $(b, -a, c)$. Lastly, a permitted origin shift $(x + \frac{1}{2}, y, z)$ was applied.

B2. Difference tables (Table 2)

For pairwise comparisons of crystal structures we calculated the absolute value of the difference between the relative atomic coordinates from the two structures, *e.g.* $\Delta(x/a) = |(x/a)_1 - (x/a)_2|$. In addition, we multiplied these relative differences with the corresponding unit-cell lengths of ludwigite in order to obtain absolute values on a common scale, *e.g.* $\Delta x = \Delta(x/a) \cdot a_{\text{ludwigite}}$. In contrast to Fig. 5, the first two columns corresponding to the 'extra' metal sites are omitted because they are uninformative due to their symmetry restricted coordinates and unoccupied in malachite and rosasite.

B3. MRA structure model (Fig. 5, bottom)

The MRA model presented here is obtained by averaging corresponding malachite and rosasite values within the restrictions of the higher symmetry. It should be noted that the first two site columns do not correspond directly to their counterparts in the other tables of Fig. 5. The unoccupied sites corresponding to the 'additional' metal atoms of the ludwigite family are omitted and the space is used to list the two hydrogen sites, which are based on the malachite data.

References

Bärnighausen, H. (1980). *Match*, **9**, 139–175.
Behrens, M. (2009). *J. Catal.* **267**, 24–29.
Behrens, M. & Girgsdies, F. (2010). *Z. Anorg. Allg. Chem.* **636**, 919–927.
Behrens, M., Girgsdies, F., Trunschke, A. & Schlögl, R. (2009). *Eur. J. Inorg. Chem.* **10**, 1347–1357.

Table 2
Difference table.

Malachite–ludwigite	M	M	O	O	O	O	O	C/B
$\Delta(x/a)$	0.004	0.008	0.007	0.015	0.016	0.006	0.018	0.008
$\Delta(y/b)$	0.008	0.008	0.007	0.006	0.013	0.006	0.001	0.001
$\Delta(z/c)$	0.108	0.112	0.140	0.081	0.131	0.158	0.050	0.027
Δx (Å)	0.04	0.07	0.06	0.14	0.15	0.06	0.17	0.07
Δy (Å)	0.10	0.10	0.09	0.07	0.16	0.07	0.01	0.01
Δz (Å)	0.33	0.34	0.42	0.24	0.40	0.48	0.15	0.08

Rosasite–ludwigite	M	M	O	O	O	O	O	C/B
$\Delta(x/a)$	0.001	0.010	0.001	0.014	0.005	0.017	0.008	0.001
$\Delta(y/b)$	0.010	0.009	0.004	0.004	0.009	0.007	0.006	0.001
$\Delta(z/c)$	0.028	0.116	0.093	0.061	0.133	0.011	0.099	0.117
Δx (Å)	0.01	0.09	0.01	0.13	0.05	0.16	0.07	0.01
Δy (Å)	0.12	0.11	0.05	0.05	0.11	0.09	0.07	0.01
Δz (Å)	0.08	0.35	0.28	0.18	0.40	0.03	0.30	0.35

$Cu_2AlO_2BO_3$–ludwigite	M	M	O	O	O	O	O	B
$\Delta(x/a)$	0.009	0.009	0.003	0.004	0.007	0.008	0.020	0.009
$\Delta(y/b)$	0.000	0.002	0.002	0.002	0.005	0.009	0.002	0.004
$\Delta(z/c)$	0.040	0.071	0.002	0.041	0.017	0.005	0.087	0.035
Δx (Å)	0.08	0.09	0.02	0.03	0.07	0.08	0.18	0.08
Δy (Å)	0.00	0.02	0.03	0.02	0.06	0.11	0.03	0.05
Δz (Å)	0.12	0.22	0.01	0.12	0.05	0.01	0.26	0.11

$Cu_2AlO_2BO_3$–malachite	M	M	O	O	O	O	O	B/C
$\Delta(x/a)$	0.005	0.001	0.010	0.012	0.009	0.014	0.002	0.001
$\Delta(y/b)$	0.008	0.010	0.009	0.004	0.018	0.003	0.003	0.005
$\Delta(z/c)$	0.148	0.183	0.142	0.122	0.114	0.163	0.137	0.062
Δx (Å)	0.05	0.01	0.09	0.11	0.08	0.13	0.02	0.01
Δy (Å)	0.10	0.12	0.11	0.05	0.22	0.04	0.04	0.06
Δz (Å)	0.45	0.55	0.43	0.37	0.34	0.49	0.41	0.19

Belsky, A., Hellenbrandt, M., Karen, V. L. & Luksch, P. (2002). *Acta Cryst.* B**58**, 364–369.

Bems, B., Schur, M., Dassenoy, A., Junkes, H., Herein, D. & Schlögl, R. (2003). *Chem. Eur. J.* **9**, 2039–2052.

Bergerhoff, G. (2001). *Z. Anorg. Allg. Chem.* **627**, 2075–2080.

Bergerhoff, G., Berndt, M., Brandenburg, K. & Degen, T. (1999). *Acta Cryst.* B**55**, 147–156.

Bergerhoff, G. & Brown, I. D. (1987). *Crystallographic Databases*, edited by F. H. Allen, G. Bergerhoff and R. Sievers, pp. 77–95. Chester: International Union of Crystallography.

Bluhm, K. & Müller-Buschbaum, Hk. (1989a). *Monatsh. Chem.* **120**, 85–89.

Bluhm, K. & Müller-Buschbaum, Hk. (1989b). *Z. Anorg. Allg. Chem.* **575**, 26–30.

Bordet, P. & Suard, E. (2009). *Phys. Rev. B*, **79**, 144408.

Buerger, M. J. (1947). *J. Chem. Phys.* **15**, 1–16.

Crystal Impact (2006). *DIAMOND*. Crystal Impact GbR, Bonn, Germany.

Dickens, P. G., Stuttard, G. P. & Patat, S. (1993). *J. Mater. Chem.* **3**, 339–341.

Erdös, E. & Altorfer, H. (1976). *Werkst. Korros.* **17**, 304–312.

Hriljac, J. A., Brown, R. D., Cheetham, A. K. & Satek, L. C. (1990). *J. Solid State Chem.* **84**, 289–298.

Irwin, M. B. & Peterson, R. C. (1999). *Can. Mineral.* **37**, 939–943.

Ivantchev, S., Kroumova, E., Madariaga, G., Pérez-Mato, J. M. & Aroyo, M. I. (2000). *J. Appl. Cryst.* **33**, 1190–1191.

Lima-de-Faria, J., Hellner, E., Liebau, F., Makovicky, E. & Parthé, E. (1990). *Acta Cryst.* A**46**, 1–11.

Liu, Y., Qin, S., Li, H., Li, X., Li, Y. & Liu, J. (2009). *Acta Geol. Sinica*, **83**, 615–617.

Looijenga-Vos, A. & Buerger, M. J. (2006). *International Tables for Crystallography*, Vol. A, 1st online ed., edited by Th. Hahn, pp. 44–54. Chester: International Union of Crystallography [doi: 10.1107/97809553602060000100].

Megaw, H. D. (1973). *Crystal Structures: A Working Approach.* Philadelphia: Saunders.

Millar, G. J., Holm, I. H., Uwins, P. J. R. & Drennan, J. (1998). *J. Chem. Soc. Faraday Trans.* **94**, 593–600.

Mir, M., Janczak, J. & Mascarenhas, Y. P. (2006). *J. Appl. Cryst.* **39**, 42–45.

Müller, U. (2004). *Z. Anorg. Allg. Chem.* **630**, 1519–1537.

Müller, U. (2006). *International Tables for Crystallography*, Vol. A1, 1st online ed., edited by H. Wondratschek & U. Müller, pp. 428–722. Chester: International Union of Crystallography [doi: 10.1107/97809553602060000101].

Parthé, E. & Gelato, L. M. (1984). *Acta Cryst.* A**40**, 169–183.

Pekov, I. V., Perchiazzi, N., Merlino, S., Kalachev, V. N., Merlini, M. & Zadov, A. E. (2007). *Eur. J. Mineral.* **19**, 891–898.

Perchiazzi, N. (2006). *Z. Kristallogr.* **23**, 505–510.

Perchiazzi, N. & Merlino, S. (2006). *Eur. J. Mineral.* **18**, 787–792.

Porta, P., De Rossi, S., Ferraris, G., Lo Jacono, M., Minelli, G. & Moretti, G. (1988). *J. Catal.* **109**, 367–377.

Roberts, A. C., Jambor, J. L. & Grice, J. D. (1986). *Powder Diffr.* **1**, 56–57.

Schaefer, J. & Bluhm, K. (1994). *Z. Allg. Anorg. Chem.* **620**, 1578–1582.

116   Girgsdies and Behrens · Structural relations of malachite. I

Acta Cryst. (2012). B**68**, 107–117

Schaefer, J. & Bluhm, K. (1995). *Z. Allg. Anorg. Chem.* **621**, 571–575.

Siegel, S., Viste, A., Hoekstra, H. R. & Tani, B. (1972). *Acta Cryst.* **B28**, 117–121.

Spek, A. L. (2009). *Acta Cryst.* **D65**, 148–155.

Süsse, P. (1967). *Acta Cryst.* **22**, 146–151.

Waller, D., Stirling, D., Stone, F. S. & Spencer, M. S. (1989). *Faraday Discuss. Chem. Soc.* **87**, 107–120.

Wells, A. F. (1951). *Acta Cryst.* **4**, 200–204.

Wondratschek, H. & Aroyo, M. I. (2006). *International Tables for Crystallography*, Vol. A1, 1st online ed., edited by H. Wondratschek & U. Müller, pp. 42–58. Chester: International Union of Crystallography [doi: 10.1107/97809553602060000101].

Zigan, F., Joswig, W. & Schuster, H. D. (1977). *Z. Kristallogr.* **145**, 412–426.